Unraveling the mechanism behind air instability in thin semiconducting polymer layers p-doped with molybdenum dithiolene complexes

Tamara Nunes Domschke, Olivier Bardagot, Anass A Benayad, Renaud Demadrille, Alexandre Carella, Raphael Clerc, Alexandre Pereira

Article type: Research Paper

Unraveling the Mechanism Behind Air Instability in Thin Semiconducting Polymer Layers p-Doped with Molybdenum Dithiolene Complexes

Tamara Nunes Domschke, Olivier Bardagot, Anass Benayad, Renaud Demadrille, Alexandre Carella, Raphael Clerc and Alexandre Pereira**

T. Nunes Domschke, Dr. A. Benayad, Dr. A. Carella, Dr. A. Pereira
University Grenoble Alpes, CEA, LITEN, DTNM, F-38054 Grenoble, France
E-mail: alexandre.pereira@cea.fr
Dr. O. Bardagot, Dr. R. Demadrille
University Grenoble Alpes, CEA, CNRS, IRIG, SyMMES, F-38000 Grenoble, France
Prof. Raphael Clerc
UJM-Saint-Etienne, Institut d'Optique Graduate School, Laboratoire Hubert Curien UMR 5516, F-42000 Saint-Etienne, France
E-mail: raphael.clerc@institutoptique.fr

Keywords: molecular p-type doping, air stability, organic semiconductors, degradation

Abstract

Doping efficiency and stability are crucial requirements for the integration of doped organic semiconductors in optoelectronic devices. This work presents a detailed experimental study on the air stability of p-doped systems based on a low-bandgap polymer, poly[(4,8-bis-(2-ethylhexyloxy)-benzo(1,2-b:4,5-b')dithiophene)-2,6-diyl-alt-(4-(2-ethylhexanoyl)-thieno[3,4-b]thiophene-)-2-6-diyl) (PBDTTT-c) doped with a strong molecular p-dopant, i.e. molybdenum tris[1-(trifluoroethanoyl)-2-(trifluoromethyl) ethane-1,2-dithiolene] (Mo(tfd-$COCF_3)_3$). The electrical conductivity and the optical absorption are measured for different dopant concentrations in argon atmosphere, and their variations monitored as a function of the air exposure time. The results indicate a clear instability under ambient air related to a dedoping process, which is particularly pronounced in ultra-thin (< 50 nm) doped layers. By evaluating the stability of the p-doped polymer layers under different atmospheres (ambient air, anhydrous air and argon), the detrimental impact of moisture and/or $O_2(H_20)_n$ complexes is highlighted. X-ray Photoelectron Spectroscopy (XPS) revealed that the p-doping instability

in ambient air can be assigned to changes in the oxidation state of the metallic center as well as to an intrinsic degradation of the dopant molecule. This study unravels an important degradation mechanism with this class of dopants that should be taken under consideration and solved for future integration of ultrathin p-doped layers in printed electronic devices.

1. Introduction

Organic semiconductors (OSCs) are promising materials for low-cost,[1] flexible,[2] large-area[3] production of printed electronic devices. These materials can be employed in their semi-conducting state as active layers in organic field effect transistors (OFETs),[4] light-emitting diodes (OLEDs)[5] and organic photovoltaics (OPVs).[6–8] They are also employed in their doped state as interfacial layers in optoelectronic devices, to favor the extraction/injection of charges[9,10] or in thermoelectric devices.[11,12] In this context, the development of an efficient and stable doping process is an important research topic. Molecular doping is a powerful tool to tune the electrical properties of OSCs, offering the possibility to improve the performance of various organic optoelectronic devices.[9,13,14] By blending dopant molecules with high electron affinities (EA), *i.e.* low-lying LUMO levels (p-dopants), or low ionization energies (IE), *i.e.* high-lying HOMO levels (n-dopants) with an OSC, it is possible to increase the electrical conductivity by several orders of magnitude[15–17] and to tailor the energy levels of the host material.[18,19] Over the last years, the research in this field has focused on the fundamental understanding of the doping mechanisms as well as on the development of processing condition allowing to control the doping efficiency in OSCs.[20–23] However, the stability and degradation mechanisms occurring in p-doped OSCs received little attention, although it is a crucial aspect for the future integration of these materials into printed devices.

Nonetheless, it is well-known that organic electronic devices can undergo chemical reactions with oxygen and/or water, leading to significant performance loss over time when exposed to

ambient conditions.[24–26] Organic materials are considered to be kinetically air-stable if their EA is below the electron traps from oxygen and water related species, *i.e.* below 4.0 eV.[27–30] This criterion is especially challenging for n-doped OSCs, given the low IE of efficient molecular n-dopant and also the low EA of the anion host.[12,31] By exposing different OSCs to ambient air, recent studies identified a common deep-lying electron trap around -3.6 eV that was associated to the presence of $O_2(H_20)_2$ hydrated oxygen complexes.[29,30,32] In this context, Tietze *et al.* showed that the n-doping effect, after short periods of air exposure, remained partially active in organic host molecules with EA higher than -3.6 eV.[30,31]

Contrary to n-type dopants, molecular p-dopants are usually considered as air-stable materials, since their LUMO levels lye far below -4.0 eV. To the best of our knowledge, there are no studies investigating the air stability of p-doped OSCs. In the literature, p-doped layers are mostly processed under inert atmosphere (or vacuum), which obviously tends to minimize the risk of air-related degradation mechanisms. Still, air stability is an important requirement for the compatibility of p-doped OSCs with printed electronics, as many real device applications require thin doped layers (<100 nm) processed in air.

Here, we present a thorough investigation of the air stability of p-doped OSCs. For this study, we chose Poly[(4,8-bis-(2-ethylhexyloxy)-benzo(1,2-b:4,5-b')dithiophene)-2,6-diyl-alt-(4-(2-ethylhexanoyl)-thieno[3,4-b]thiophene-)-2-6-diyl)] (PBDTTT-c), which is one of the new generation donor polymers developed for OPV applications,[6,7] and molybdenum tris[1-(trifluoroethanoyl)-2-(trifluoromethyl) ethane-1,2-dithiolene] ($Mo(tfd\text{-}COCF_3)_3$), as a dopant. This dopant belongs to a popular class of molecules, specifically developed for the doping of organic p-type semiconductors and presents higher solubility compared to previously reported Mo-based dopants, such as $Mo(tfd)_3$.[33] Recent studies have already confirmed good p-doping electrical properties for PBDTTT-c:$Mo(tfd\text{-}COCF_3)_3$ layers and investigated the doping mechanisms in this system.[34–36]

After characterizing the conductivity and UV-Vis-NIR absorption of freshly prepared PBDTTT-c:Mo(tfd-$COCF_3)_3$ layers, we showed that their doping characteristics are not stable in ambient conditions. By performing a stability study under different atmospheres, we highlighted the negative impact of air humidity on the p-doping stability of PBDTTT-c:Mo(tfd-$COCF_3)_3$ layers. This observation was extended to Mo(tfd-$COCF_3)_3$-doped poly(3-hexylthiophene) (P3HT) layers, indicating that the observed instability is independent of the polymer host. X-ray photoemissions spectroscopy (XPS) revealed significant changes in the dopant molecule and in the oxidation state of the metal center after air exposure.

2. Experimental

2.1. Materials

PBDTTT-c (PDI: 1.8-2.5, Mn > 23 kDa) was purchased from Solarmer and P3HT (regiorandom) and o-Xylene (anhydrous, 97 %) were purchased from Sigma-Aldrich. All materials were used as received without further purification.

2.2. Sample fabrication

PBDTTT-c (5.5 – 40 g L^{-1}, o-Xylene), P3HT (5.5 g L^{-1}, o-Xylene), Mo(tfd-$COCF_3)_3$ (2.0 g L^{-1}, o-Xylene) solutions were stirred overnight at room temperature. Immediately before spin-coating, the appropriated amount of dopant solution (depending on the desired doping level) is added to the polymer solution. The doping concentration is given in mol%, *i.e.* number of dopant molecules per monomer unit of polymer. For PBDTTT-c:Mo(tfd-$COCF_3)_3$, the final polymer concentration varied between 4.7-19 g L^{-1}, depending on the desired layer thickness (between 15-200 nm). For P3HT: Mo(tfd-$COCF_3)_3$, only 15 nm-thick layers were considered. Glass slides for UV-Vis-NIR spectroscopy were cleaned by sequential sonication steps in acetone (10 min) and isopropanol (10 min), and dried under argon stream. For electrical measurements, XPS analysis, and EPR measurements gold-coated poly(ethylenenaphthalate) (PEN) substrates were patterned using photolithography and cleaned by sonication in an

acetone bath (10 min). The spin-coating speeds were varied between 500-1000 rpm, depending on the solution concentration and the desired layer thickness. The complete sample preparation was performed in an argon-filled glovebox (<5 ppm H_2O, O_2) equipped with a molecular sieve solvent trap. The thickness of samples was determined using a TOHO FP-10 contact profiler.

2.3. Characterization methods

The transmission line method (TLM) was used to measure the conductivity of the doped layers. The patterned flexible PEN (12 µm) /gold (30 nm) substrates presented a channel width of *ca.* 14,500 µm and a channel length varying from 50 to 1000 µm. Current-voltage (I-V) measurements were performed in the dark and inside the argon-filled glovebox with a Keithley 2400 SourceMeter. The conductivity was determined from the ohmic region of the I-V curves. An identical setup was used for the measurement under ambient air. To characterize the stability of the electrical conductivity under ambient air, freshly prepared samples were exposed to air (dark) and their I-V curves were automatically collected every five minutes, for a chosen channel length. The results are plotted in conductance versus time.

A PerkinElmer Lambda 950 spectrophotometer with integrating sphere was used to measure the UV-Vis-NIR absorption spectrum of the solid samples. Total transmission and total reflection were measured to obtain the total absorption. The UV-vis-NIR measurements were performed under ambient atmosphere. The samples were measured directly after leaving the glovebox, limiting the air exposure to a few minutes.

Cyclic voltammetry (CV) measurements were performed with a three-electrode setup, consisting of a platinum electrode as a working electrode (ALS, diameter 1 mm), a platinum wire as counter electrode, and a non-aqueous $Ag/AgNO_3$ electrode as pseudo-reference. PBDTTT-c measurements were performed in freshly distilled acetonitrile and $Mo(tfd\text{-}COCF_3)_3$ in freshly distilled THF. Tetrabutylammonium hexafluorophosphate is used as supporting electrolyte (NBu_4PF_6, Electrochemical grade, Sigma Aldrich, 0.1 M), dried under

primary vacuum at room temperature. The dopant was analyzed in solution (2 mM) and the polymer was drop-casted on the working electrode (from 4.7 $g.L^{-1}$ solution in o-Xylene) and analyzed as a film. The voltammograms were recorded at a scan rate of 50 $mV.s^{-1}$ and calibrated with respect to the half-wave oxidation potential of ferrocene (Fc^+/Fc),. The electron affinities of dopants and their anions were calculated using E_{EA} (eV) ≈ 4.8 + E_{red}^{onset}(V vs Fc^+/Fc).[37] The ionization energy of the polymer was calculated using E_{IE} (eV) ≈ 4.8 + E_{ox}^{onset} (V vs Fc^+/Fc).

X-ray photoelectron spectroscopy (XPS) analysis were performed with a ULVAC PHI 5000 VersaProbe II spectrometer using an AlKα X-ray radiation (1,486.6 eV). The residual pressure inside the analysis chamber was of 7×10^{-8} Pa. A fixed analyzer pass energy of 23 eV was used for core level scans, leading to an overall energy resolution of 0.6 eV. Survey spectra were captured at a pass energy of 117 eV. All spectra were referenced against an internal signal, typically by adjusting the C 1s level peak at a binding energy of 284.6 eV. A specific four contacts sample holder manufactured by ULVAC-PHI was used to probe the stability of thin doped layers under Ultra High Vacuum condition. The XPS spectra were fitted using the casaXPS software in which a Shirly background is assumed and the fitting peaks of the experimental spectra are defined by a combination of Gaussian (80%) and Lorentzian (20%) distribution.

Electron paramagnetic resonance (EPR) spectra were recorded with a Bruker EMX spectrometer operating at X-band frequency with an ER-4116 dual mode cavity. The measurements were done at room temperature and obtained with the following parameters: 9.655 GHz frequency, 31.65 mW power, and 3.0 G modulation amplitude. To allow a direct comparison and avoid morphology variation due to the substrate, the EPR sample is a cutout part of TLM flexible devices inserted in a 3 mm internal diameter quartz EPR tube. The film is deposited by spin-coating. PEN does not give any EPR signal in the given conditions.

3. Results and discussion

3.1. p-doping of PBDTTT-c with Mo(tfd-COCF$_3$)$_3$

The redox potentials of PBDTTT-c and Mo(tfd-COCF$_3$)$_3$ were measured with cyclic voltammetry (**Figure 1a**). The reduction of the dopant occurs *via* two, remarkably stable and reversible, one-electron transfers.[38] Such electrochemical stability of the anion and dianion species are valuable for long-lasting operations. The successive reduction waves were assigned to the LUMO and LUMO +1 levels, calculated at *ca.* -5.3 eV and -4.5 eV, respectively. For PBDTTT, the reduction and oxidation waves also presented electrochemically stable and reversible processes, with a HOMO level at *ca.* -5.1 eV and the LUMO level at *ca.* -3.1 eV. Assuming the absence of intermolecular electrostatic interactions,[39] the energy level offset between the HOMO of PBDTTT-c (≈ -5.1 eV) and the LUMO of Mo(tfd-COCF$_3$)$_3$ (≈ -5.3 eV) should favor an efficient electrical doping in this polymer:dopant system (**Figure 1b**).

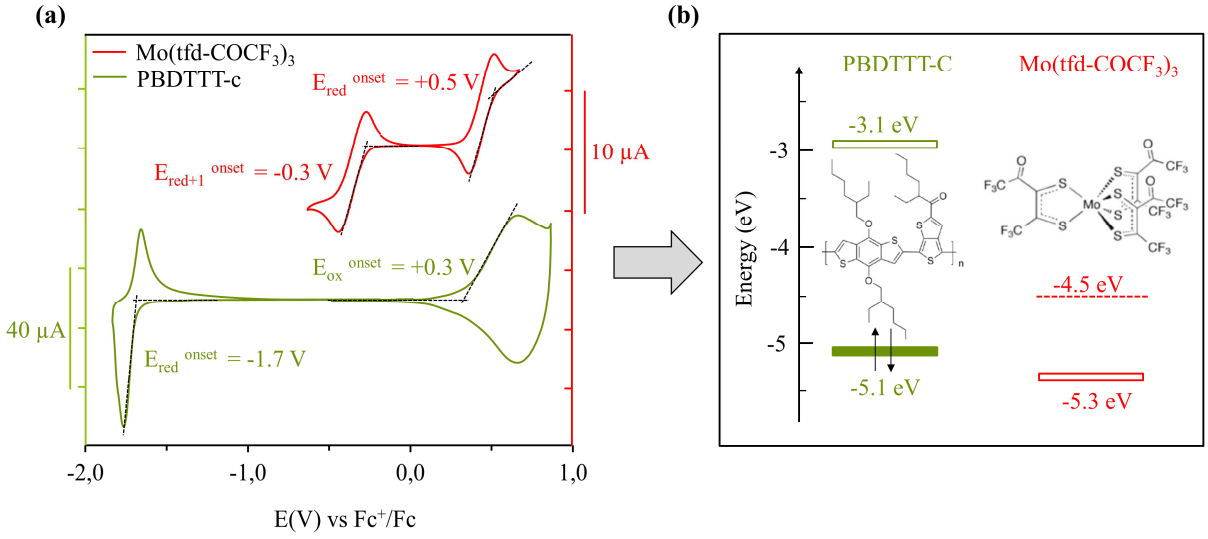

Figure 1 – (a) Cyclic voltammograms of Mo(tfd-COCF$_3$)$_3$ (in THF) and PBDTTT-c (in acetonitrile). Experimental conditions: scan rate 50mV.s^{-1}, 0.1 M [NBu$_4$][PF$_6$], 0.01 M Ag/AgNO$_3$ calibrated Fc$^+$/Fc. (b) Corresponding energy diagram with the calculated energy levels. Filled bars indicate HOMO level, unfilled bars indicate LUMO levels and dotted line indicate LUMO+1 level (See experimental section for details).

The conductivity and UV-Vis-NIR absorption spectra of freshly prepared PBDTTT-c:Mo(tfd-$COCF_3)_3$ layers were measured as a function of the dopant concentration, varying from 1 mol% to 30 mol% (1.2 wt% and 36.3 wt%). Regarding the blend solution, the final polymer concentration was kept constant at 4.7 g L^{-1}, whereas the final dopant concentration varied between 0.3 g L^{-1} and 1.6 g L^{-1}. All the samples presented a layer thickness of *ca.* 15 nm. Pristine polymer layers exhibited low conductivity of 4 x 10^{-8} S cm^{-1}, which is consistent with the low carrier density expected from neutral polymers.[40] In **Figure 2a**, the conductivity of PBDTTT-c layers is presented as a function of the Mo(tfd-$COCF_3)_3$ concentration. Compared to previous studies on the same polymer:dopant system, our samples presented exceptionally high conductivities.[34–36] The main difference between our processing conditions and those reported previously for PBDTTT-c:Mo(tfd-$COCF_3)_3$ layers relies on the absence of post-deposition thermal treatment. Having noticed its negative impact over the conductivity, our samples were measured as-cast (Figure S1). For F_4TCNQ-doped OSCs, recent articles have reported on thermally induced dedoping, which was mostly attributed to the dopant desorption.[15,41,42]

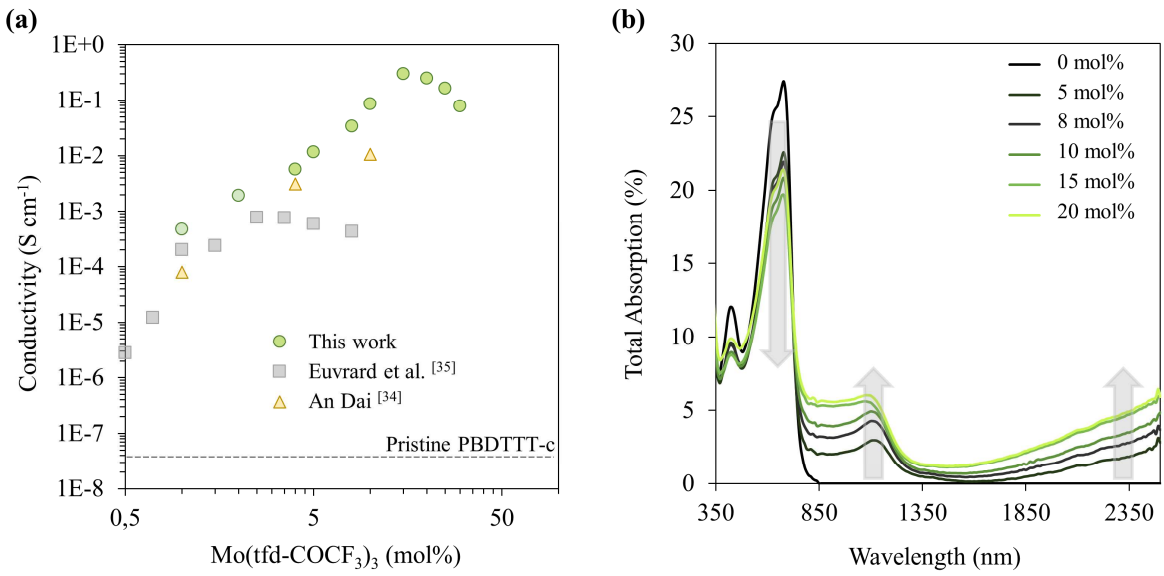

Figure 2 – Electrical conductivity as a function of the dopant concentration for PBDTTT-c:Mo(tfd-$COCF_3)_3$ layers: comparison with values published in the literature (a). UV-Vis-NIR spectra for pristine PBDTTT-c and doped PBDTTT-c:Mo(tfd-$COCF_3)_3$ layers (b).

A conductivity increase of seven orders of magnitude was observed for PBDTTT-c:Mo(tfd-$COCF_3)_3$ layers, with a maximum of 0.3 S cm^{-1} at 15 mol% Mo(tfd-$COCF_3)_3$ **(Figure 2a)**. The saturation beyond a certain dopant concentration was already reported for other doped OSCs and correlated to the limited number of dopant anions that can be accommodated in the host material, depending on the nature of the polymer-dopant interactions.[16,17,43] Therefore, the slight conductivity decrease observed above 15 mol% of Mo(tfd-$COCF_3)_3$ suggests an increase of molecular disorder due to an excess of dopant.[44]

In order to get insight on the morphology evolution of PBDTTT-c layers with the addition of Mo(tfd-$COCF_3)_3$, we compared the surface morphology of pristine and doped layers by tapping-mode atomic force microscopy (AFM) (Figure S2) and the bulk molecular order by grazing-incident wide-angle X-ray scattering (GIWAXS) (Figure S3). No significant modification of the diffractograms are observed upon doping. The addition of Mo(tfd-$COCF_3)_3$ up to 20 mol % reinforced the amorphous character of the PBDTTT-c polymer. The AFM topography indicated no drastic change in the morphology of PBDTTT-c layers up to 10 mol% Mo(tfd-$COCF_3)_3$. However, for dopant concentrations above 15 mol%, the surface morphology changes significantly.

Figure 2b reports the UV-Vis-NIR spectra for pristine PBDTTT-c and doped PBDTTT-c:Mo(tfd-$COCF_3)_3$ layers. The UV-Vis-NIR absorption spectra indicate that new sub-gap absorption bands located at 1100 nm and beyond 2000 nm appear as the Mo(tfd-$COCF_3)_3$ molar ratio is increased. This variation is concomitant with a bleaching of the PBDTTT-c π-π^* band at ~650 nm. The absorption bands in the NIR are attributed to sub-gap transitions from and to polaronic levels, evidencing an effective doping.[45–47] Above 15 mol% Mo(tfd-$COCF_3)_3$, the absorption spectra shows no significant changes, indicating that no more doped PBDTTT-c segments are formed at higher dopant concentration, in accordance with the conductivity measurements. As the neutral and ionized absorption signatures of Mo(tfd-$COCF_3)_3$ extensively overlap with the PBDTTT-c ground state absorption feature,[48,49] it is

not possible to identify the corresponding molar fraction of neutral and ionized dopant molecules, as commonly done for the F4TCNQ doped systems.[50]

3.2. Impact of air exposure on the doping characteristics

After characterizing the initial optoelectronic properties of PBDTTT-c:Mo(tfd-$COCF_3$)$_3$ layers using conductivity measurements and UV-Vis-NIR absorption spectroscopy, we investigated the doping stability under ambient air. For this study, we considered different layer thicknesses. The layer thickness of p-doped OSCs can vary considerably in the literature, depending on the processing conditions, on the characterization techniques and/or on the targeted device.[15,51–54] In terms of stability, Oh et al. have shown that for n-channel organic thin-film transistors, the ambient stability increased significantly with the layer thickness.[55] Thus, a particular attention was given to this parameter. The dopant molar ratio was fixed at 5 mol% (*i.e.* 5.9 wt%) and samples with four different layer thickness (15 nm, 45 nm, 100 nm and 200 nm) were prepared by varying the concentration of PBDTTT-c (4.7 g L^{-1}, 10.0 g L^{-1}, 14.8 g L^{-1} and 19.5 g L^{-1}, respectively).

The initial conductivity of all freshly-prepared PBDTTT-c:Mo(tfd-$COCF_3$)$_3$ layers was *ca.* 1.5 x 10^{-2} S cm^{-1}. The impact of air exposure was investigated by monitoring the conductance (see experimental section for details) and the UV-Vis-NIR spectra evolution over time (in the dark). All the samples presented a degradation of the doping characteristics upon air exposure, evidenced by a conductance decrease combined with a decrease of the NIR absorption bands and a recovery of the pristine PBDTTT-c π-π*-absorption band (**Figure 3a,b**). Moreover, Figure 3a clearly shows that the current loss upon air exposure is faster for thinner layers. This result highlights the strong influence of the layer thickness on the degradation kinetics. One possible explanation would be the diffusion of oxygen and water into PBDTTT-c layers, as observed for n-channel organic thin-film transistors.[55] As a result, considering samples with similar thickness is crucial for relevant comparative degradation studies. For comparison

purpose, we measured the conductance evolution of a pristine PBDTTT-c under the same conditions. Contrary to doped layers, the latter presented a conductance increase (close to one order of magnitude) with air exposure, which can be attributed to oxygen doping (Figure S4).[56]

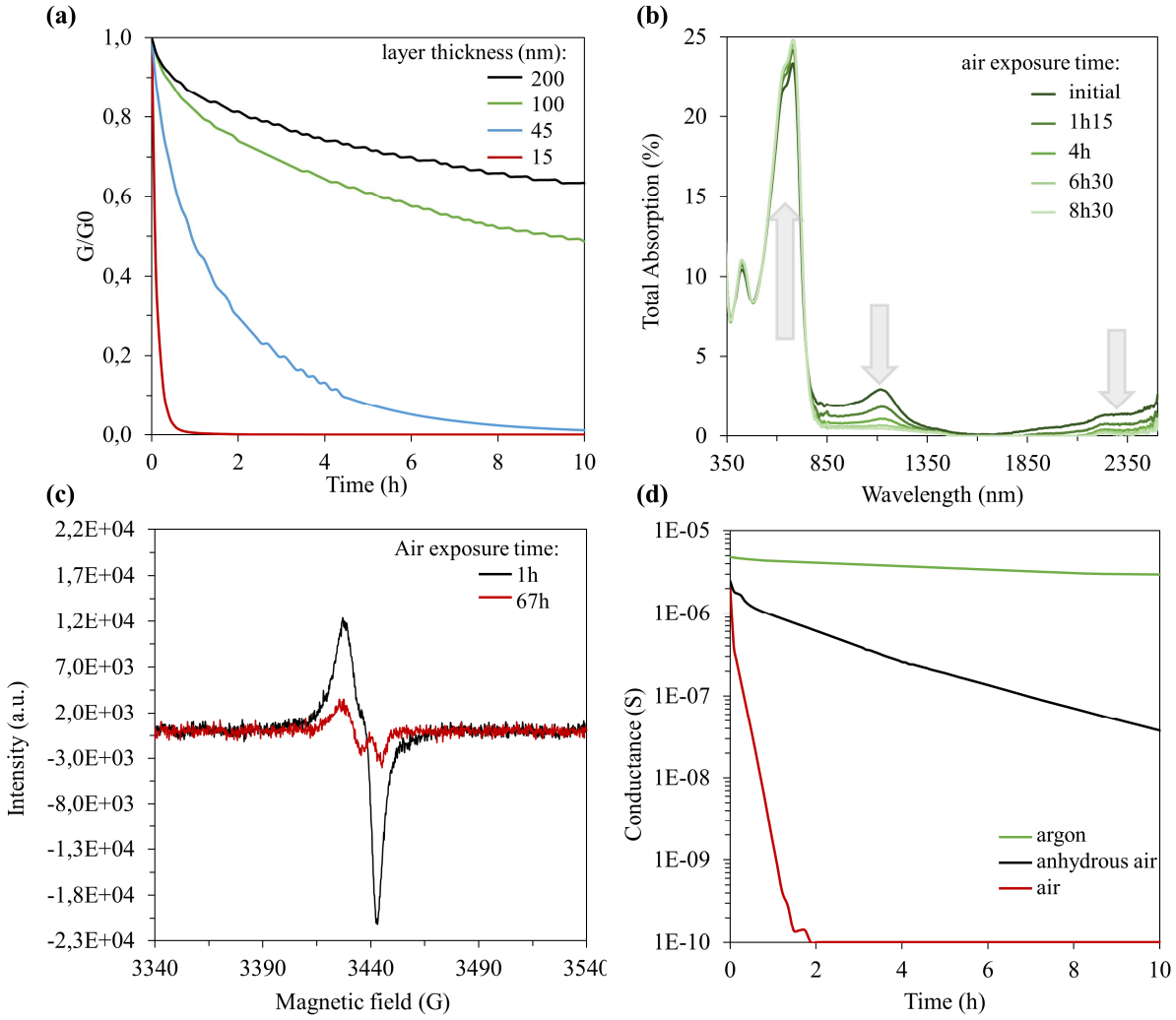

Figure 3 –Doping signatures of PBDTTT-c : $Mo(tfd\text{-}COCF_3)_3$ layers at 5 mol% under air exposure. Relative conductance (G/G_0) for layers of different thicknesses (a), UV-Vis-NIR spectra evolution for a 15 nm layer (b), EPR spectra for a 100 nm layer after 1h (black line) and 67h (red line) air exposure (c) and conductance evolution for 15 nm layers under different atmospheres (d).

The degradation spectroscopic signatures of PBDTTT-c:$Mo(tfd\text{-}COCF_3)_3$ layers suggest a dedoping mechanism upon air exposure. We confirmed this result by EPR spectroscopy. **Figure 3c** shows the EPR spectrum of a 100 nm thick sample measured after 1h and 67h air

exposure. The strong signal measured at room temperature is characteristic of organic radicals ($g \approx 2.0$) and reflects an efficient charge generation upon doping. Upon air exposure (67h, dark), the intensity of the signal is significantly decreased. The relative loss of unpaired electrons is estimated to be 83 %, as calculated from the double integration of the signals (Figure S5). Note that bipolarons, as diamagnetic species, cannot be probed by EPR measurement. This result is in accordance with the conductivity loss and the UV-Vis-NIR dedoping signatures observed upon air exposure.

Jacobs *et al.* reported on chemical mechanisms for dedoping p-doped OSCs by exposing p-doped films to electron donors with IE low enough to reduce the OSCs to its neutral state.[57] This approach was efficiently demonstrated for P3HT:F4TCNQ films, by selecting amines with adapted energy levels. In our case, PBDTTT-c:Mo(tfd-$COCF_3)_3$ layers are exposed to ambient conditions, *i.e.* water and/or molecular oxygen species present in air. Therefore, to gain deeper insights into the impact of water and oxygen on the doping stability of PBDTTT-c:Mo(tfd-$COCF_3)_3$ layers, we performed ageing experiments under different atmospheres: ambient air, anhydrous air (<200 ppm H_2O) and argon (<5 ppm H_2O and O_2). Since thinner samples presented faster degradation kinetics, this study was performed on 15 nm-thick doped layers with 5 mol% of Mo(tfd-$COCF_3)_3$.

The sample exposed to anhydrous air presented a much slower current degradation than the one exposed to ambient air **(Figure 3d)**. Under argon atmosphere, the current exhibited only a slight decrease in the considered timescale. From these results, we can affirm that moisture or hydrated oxygen complexes ($O_2(H_2O)_n$ have an important role in the p-doping instability observed in ambient air. We verified if the conductivity of PBDTTT-c:Mo(tfd-$COCF_3)_3$ layers is recovered when returning the sample to the glovebox or drying under secondary vacuum (2×10^{-7} mbar) overnight, as observed in the literature for n-doped organic molecules.[30,31,58] Nevertheless, no recovery of the doping characteristics was found for PBDTTT-c:Mo(tfd-$COCF_3)_3$ layers exposed to air.

In summary, a clear degradation of the doping characteristics upon air exposure was observed. Yet, AFM topography images do not indicate an obvious change in the morphology of the doped layers after air exposure (Figure S6). To rule out the influence of the polymer matrix on the p-doping instability, we replaced the PBTTT-c host polymer by rra-P3HT. Interestingly, we observed a similar instability for P3HT:Mo(tfd-$COCF_3$)$_3$ layers, evidenced by a fast decrease in conductivity and a bleaching of the polaronic absorption bands upon air exposure (Figure S7). These results suggest that the air-instability in the considered timescale originates from the dopant itself, and not from the polymer host.

Such air instability of p-doped layers may also occur in other polymer:dopant systems. For instance, Brinkmann and coworkers have recently observed unstable p-doping characteristics for thin PBTTT:$FeCl_3$ layers exposed to ambient conditions, without further explanation of the degradation mechanism.[22] Moreover, we also briefly considered the air stability to the widely studied P3HT:F4TCNQ system, and observed unstable doping characteristics under ambient air (Figure S8). It is likely that the degradation mechanism involved in these different systems are not the same (for instance F4TCNQ is a fully organic molecule without metallic center, contrary to $FeCl_3$ or Mo(tfd-$COCF_3$)$_3$). In this work, we will limit ourselves to the case of Mo(tfd-$COCF_3$)$_3$. However, these findings demonstrate that having materials with LUMO levels below -4.0 eV does not guarantees the air stability of doped layers. Degradation mechanisms are discussed in the following section.

3.3. Degradation mechanism of PBDTTT-c:Mo(tfd-$COCF_3$)$_3$ layers under air exposure

To gain insight into the mechanism behind the instability of Mo(tfd-$COCF_3$)$_3$ – doped OSCs under ambient air, we performed XPS analyses. This technique allows identifying the chemical state of elements present on a sample surface and is, therefore, a powerful tool for studying degradation mechanisms.[24,30] This study was performed using PBDTTT-c as host

material. Our choice was based on the higher conductivities of PBDTTT-c:Mo(tfd-$COCF_3$)$_3$ layers and the fact that this polymer has received less attention in the literature than P3HT.

XPS analysis were performed on PBDTTT-c: Mo(tfd-$COCF_3$)$_3$ doped layers before and after air exposure. To obtain information about the initial state of the pristine materials and to properly assign the peaks of the doped layers, pure Mo(tfd-$COCF_3$)$_3$ and PBDTTT-c were also analyzed. This section focuses on the S2p and Mo3d core level peak regions. The XPS spectra obtained for pristine and doped layers are presented in **Figure 4** and their respective binding energies summarized in **Table 1**. Details of peak fitting are given in Table S1-S3.

For the pristine PBDTTT-c, the S2p core level spectrum presented a splitting into two doublets (associated to spin-orbit coupling) at binding energy of 163.7 eV ($2p_{3/2}$) and 164.9 eV ($2p_{1/2}$), attributed to the C-S environment (Figure 4a). The lower intensity S2p doublet at higher binding energies were assigned to SOx groups. For the pure dopant molecule, the S2p core level spectrum presented doublets at 162.3 eV ($2p_{3/2}$) and 163.5 eV ($2p_{1/2}$), which were attributed to the sulfur present in the Mo-S-C environment (Figure 4b). A small fraction of S2p doublets were found at higher oxidation states assigned to $(S_n)^{2-}$ and (SO_2)-like species, which are possibly related to residual impurities from synthesis present in the material.

Regarding the 3d spectral region of Mo in the pure dopant molecule, spin-orbit coupling also induces a splitting of the Mo3d core levels into two doublets (Figure 4c, green area): a higher intensity doublet at 229.1 eV ($3d_{5/2}$) and 232.3 eV ($3d_{3/2}$), and a lower intensity one at 231.3 eV ($3d_{5/2}$) and 234.4 eV ($3d_{3/2}$). Thus, Mo atoms in the dopant molecule are present in two different oxidation states. Besides, the additional peak at 226.7 eV was assigned to the S2s core level of the dopant ($S2s_{dop}$). Comparing with the literature, the Mo3d binding energies measured for Mo(tfd)$_3$ and Mo(tfd-CO_2Me)$_3$ are similar to those measured for the higher intensity doublet of Mo(tfd-$COCF_3$)$_3$.[34,59] The authors suggested an oxidation state of 4+ for the Mo coordinates with tris(dithiolene) ligands, as the binding energies are similar to those measured for MoS_2 .[60] Therefore, we attributed the doublet at 229.1 eV ($3d_{5/2}$) and

232.3 eV ($3d_{3/2}$) to the Mo^{4+} oxidation state and the doublet at 231.3 eV ($3d_{5/2}$) and 234.4 eV ($3d_{3/2}$) to a Mo fraction at higher oxidation state, between 4+ and 5+. The latter was not observed in the aforementioned publications.

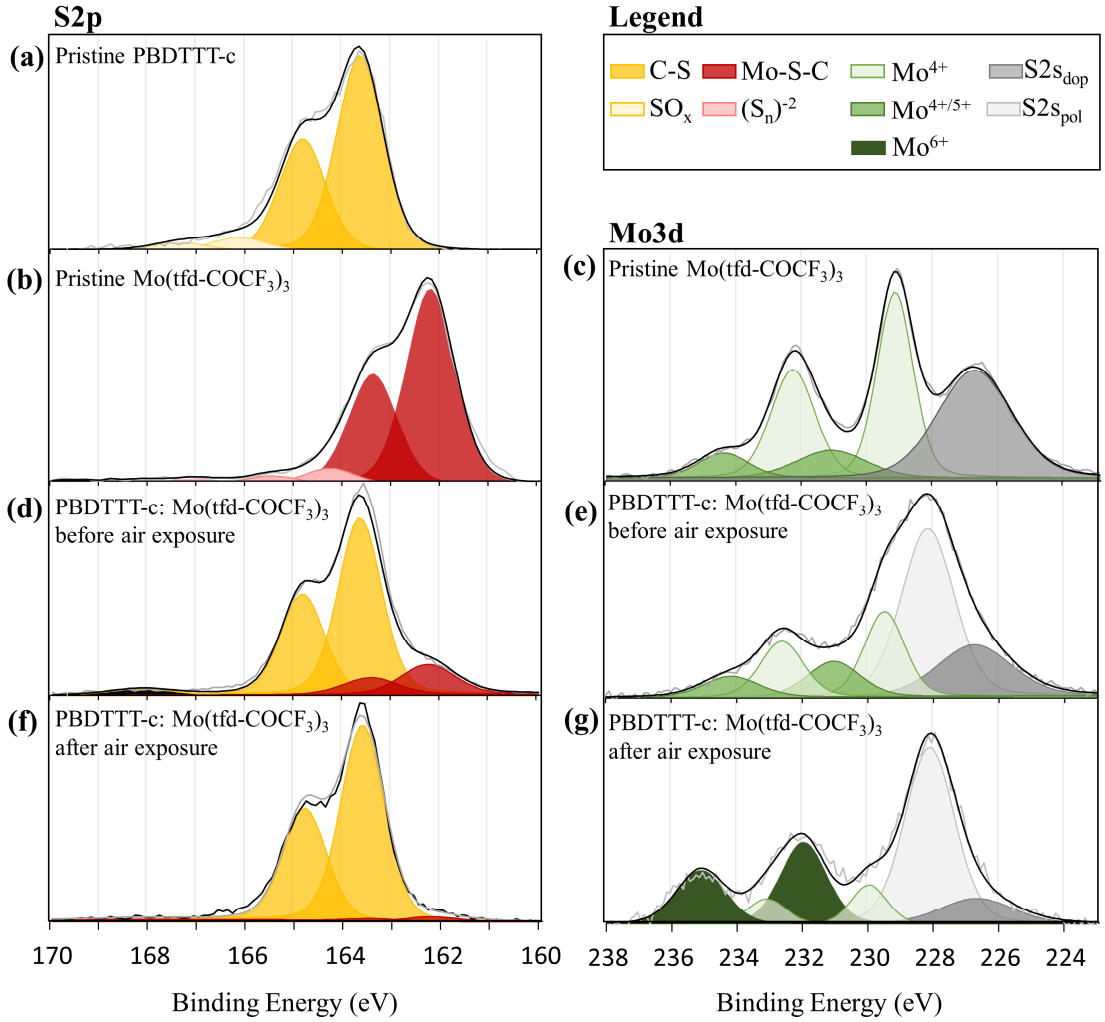

Figure 4 – Mo3d and S2p levels measured by XPS: (a) pristine PBDTTT-c, (b,c) pristine $Mo(tfd\text{-}COCF_3)_3$ and 15 nm $Mo(tfd\text{-}COCF_3)_3$-doped PBDTTT-c layer at 25 mol% (d,e) before and (f,g) after 20h air exposure.

Before performing XPS analyses on PBDTTT-c:$Mo(tfd\text{-}COCF_3)_3$ samples, we verified the stability of 15 nm doped layers in Ultra High Vacuum (UHV) at 10^{-9} mbar. Using a sophisticated sample holder, the current evolution was monitored inside the XPS UHV chamber. Only a slight decrease in conductivity was observed after 12h under UHV (Figure S9). Thus, we assumed that our doped samples are stable in the XPS measurement conditions.

For this experiment, two PBDTTT-c:Mo(tfd-$COCF_3)_3$ samples of 15 nm were freshly prepared with a dopant concentration of 25 mol%. This molar ratio was chosen to obtain a higher intensity of the dopant signal. The first sample was stored in argon atmosphere and the second was exposed to air for 20h. Both samples presented an initial conductivity of approximatively 7 x 10^{-2} S cm^{-1}. After 20h, the electrical conductivity of the sample exposed to air dropped to 7.5 x 10^{-5} S cm^{-1} whereas the one stored under argon atmosphere presented no significant change. This result is consistent with the previous ageing test.

Table 1 - XPS binding energies (eV) of Mo and S levels for pristine bulk materials (PBDTTT-c and Mo(tfd-$COCF_3)_3$) and for Mo(tfd-$COCF_3)_3$-doped PBDTTT-c layers (25 mol%, 15 nm) before and after air exposure. The main changes are highlighted in bold text.

Material	$S2s_{dop}$	$S2s_{pol}$	C-S		Mo-S-C		Mo^{4+}		$Mo^{4+/5+}$		Mo^{6+}	
			$S2p_{3/2}$	$S2p_{1/2}$	$S2p_{3/2}$	$S2p_{1/2}$	$Mo3d_{5/2}$	$Mo3d_{3/2}$	$Mo3d_{5/2}$	$Mo3d_{3/2}$	$Mo3d_{5/2}$	$Mo3d_{3/2}$
Pristine PBDTTT-c	–	–	163.7	164.9	–	–	–	–	–	–	–	–
Pristine Mo(tfd-$COCF_3)_3$	226.7	–	–	–	162.3	163.5	229.1	232.3	231.3	234.4	–	–
PBDTTT-c: Mo(tfd-$COCF_3)_3$ **before air exposure**	226.7	228.1	163.7	164.9	162.3	163.5	229.4	232.6	**231.0**	**234.1**	**–**	**–**
PBDTTT-c: Mo(tfd-$COCF_3)_3$ **after air exposure**	226.7	228.1	163.7	164.9	162.3 **(vanished)**	163.5	230.0	233.1	**–**	**–**	**232.0**	**235.1**

For the PBDTTT-c: Mo(tfd-$COCF_3)_3$ layer kept under argon atmosphere, the S2p spectral region presented the C-S environment of the polymer and Mo-S-C environment of the dopant at the same binding energies as measured for the pristine materials (Figure 4d). Regarding the Mo3d spectra region, we observed the same two doublets of the pure dopant (Figure 4e). In addition of the $S2s_{dop}$, we also observed the S2s core level of the polymer at 228.1 eV ($S2s_{pol}$). Note that no Mo doublets are observed in lower oxidation states, as one could expect for dopant molecules in its reduced state (after electron transfer from PBDTTT-c). Qi *et al.* presented DFT calculations for the $Mo(tfd)_3$ anion showing that the extra electron is mainly accommodated by the ligands and that Mo is only slightly influenced by the reduction.[59]

This behavior was observed in different molybdenum sulfide complexes, such as Chevrel phases (Mo_6S_8), used as electrode material for Mg batteries.[61] The charge transfer during the reduction process in Mo_6S_8 involves both metal and ligands, inducing structural rearrangements rather than a formal Mo reduction. Additionally, electronic structural calculations of metal dithiolene complexes revealed an extensive ligand-metal mixing of the frontier orbitals with redox-active ligands.[62] Therefore, conventional oxidation-state descriptions are not suitable in these metal complexes. This might explain why we observed the same Mo core levels for pure Mo(tfd-$COCF_3$)$_3$ and for PBDTTT-c:Mo(tfd-$COCF_3$)$_3$ layers. For the PBDTTT-c:Mo(tfd-$COCF_3$)$_3$ sample exposed to ambient air (20h), significant changes in the dopant molecule were detected (Figure 4f,g). In the Mo3d spectral region, we observed a smaller fraction of the Mo^{4+} oxidation state at slightly higher binding energies: 229.9 eV ($3d_{5/2}$) and 233.0 eV ($3d_{3/2}$). Additionally, a higher intensity doublet appeared at 231.9 eV ($3d_{5/2}$) and 235.1 eV ($3d_{3/2}$) that can be assigned to a Mo^{6+} oxidation state.[63,64] No Mo component at intermediate oxidations state was observed in this sample. Hence, upon air exposure the *d* character of the Mo atom changes from a d^2 (Mo^{4+}) to a d^0 (Mo^{6+}), *i.e.* from a conducting to an isolating electronic structure. This observation is in accordance with the observed conductivity decrease. Regarding the S2p spectral region, the peaks corresponding to Mo-S-C environment in the dopant molecule vanished after air exposure (Figure 4f, red area). In contrast, no changes were observed in the peaks assigned to the C-S environment of the polymer (Figure 4f, yellow area). Lastly, the total atomic concentration of F in the doped layers presented a significant reduction after air exposure (Figure S10).

Summing up, exposing PBDTTT-c:Mo(tfd-$COCF_3$)$_3$ layers to ambient air (dark) presented no change in the polymer core levels, contrary to the dopant molecule, which presented an oxidation of the Mo3d core levels and signs of degradation of the dopant molecule. These results strikingly indicate that Mo(tfd-$COCF_3$)$_3$ interacts with species present in ambient air (moisture and/or hydrated oxygen complexes), even though its EA (≈ 5.3 eV) is located

within the air-stability window.[27,30,32]. Dupé *et al.* observed the transition from Mo^{4+} to Mo^{6+} when studying the activation of molecular oxygen by molybdenum complexes with reduced molybdenum centers, aiming to mimic the activity of molybdenum enzymes.[65] These enzymes use mainly water as a source of oxygen.[66] Thus, the stability of neutral and ionized p-dopants to water and/or hydrated oxygen complexes might be an important requirement to achieve air-stable p-doped layers.

4. Conclusion

In this work, the air stability of $Mo(tfd\text{-}COCF_3)_3$–doped PBDTTT-c layers has been investigated in detail. When exposed to ambient air, both conductivity and UV-Vis-NIR absorptions have clearly highlighted a phenomenon of dedoping. Such air-induced dedoping was particularly pronounced in ultra-thin layers (< 50 nm), suggesting that thicker layers act as a kinetic barrier to the diffusion of ambient oxidants. A similar trend was also observed when exposing $Mo(tfd\text{-}COCF_3)_3$-doped P3HT layers to air, indicating that the observed p-doping instability is independent of the polymer host. The fact that p-doped OSCs were mainly studied under controlled atmosphere and/or in thicker layers so far may explain why this air instability has not been reported yet. By performing ageing experiments in different atmospheres (ambient air, anhydrous air, argon), moisture and/or hydrated oxygen complexes were identified as being the critical factor responsible for the p-doping instability under ambient air.

In order to further investigate the air induced dedoping mechanism, a careful XPS analysis of PBDTTT-c:$Mo(tfd\text{-}COCF_3)_3$ doped layers after air exposure has been performed. The dopant molecule showed evidences of oxidation, as well as an intrinsic degradation. We can assume that the oxidation state of $Mo(tfd\text{-}COCF_3)_3$ molecules blended with PBDTTT-c is not stable in the presence of moisture and/or oxygen hydrated complexes. Thus, the air stability of $Mo(tfd\text{-}COCF_3)_3$ – doped OSCs is mainly driven by the stability of the dopant molecule itself. This

result invites to reconsider the air stability of other polymer:p-dopant systems, even if pristine materials present energy levels in the air-stability window.

Hence, the process of p-doping OSCs under ambient conditions has to be considered with caution, especially when dealing with thin and ultra-thin p-doped layers, as required for efficient doped contacts in organic devices. For the large-scale production scenario of printed organic electronic devices, an anhydrous environment might be an envisioned solution to attenuate the instability of $Mo(tfd\text{-}COCF_3)_3$ –doped OSCs during fabrication.

Acknowledgements

The authors would like to thank Prof. Antoine Kahn (Princeton University) for providing the $Mo(tfd\text{-}COCF_3)_3$ compound and for valuable discussions, and Amélie Revaux (CEA LITEN) for her support and for helpful meetings and discussions. We would like to thank Stephanie Pouget (CEA IRIG) for the GIWAXS measurements, Serge Gambarelli (CEA IRIG) for EPR measurements, and Dennis Mariolle (CEA LETI) as well as François Saint-Antonin (CEA LITEN) for the AFM topography measurements.

References

[1] A. Gambhir, P. Sandwell, J. Nelson, The future costs of OPV – A bottom-up model of material and manufacturing costs with uncertainty analysis, Sol. Energy Mater. Sol. Cells. 156 (2016) 49–58. https://doi.org/10.1016/j.solmat.2016.05.056.

[2] X. Zhao, S.T. Chaudhry, J. Mei, Heterocyclic building blocks for organic semiconductors, Ch. 5, in: E.F.V. Scriven, C.A. Ramsden (Eds.), Advances in heterocyclic chemistry, Academic Press, 2017, 133–171. https://doi.org/10.1016/bs.aihch.2016.04.009.

[3] R.R. Søndergaard, M. Hösel, F.C. Krebs, Roll-to-Roll fabrication of large area functional organic materials, J. Polym. Sci., Part B: Polym. Phys. 51 (2013) 16–34. https://doi.org/10.1002/polb.23192.

[4] G. Horowitz, Organic Field-effect transistors, Adv. Mater. 10 (1998) 365–377. https://doi.org/10.1002/(SICI)1521-4095(199803)10:5<365::AID-ADMA365>3.0.CO;2-U.

[5] S. Reineke, F. Lindner, G. Schwartz, N. Seidler, K. Walzer, B. Lüssem, K. Leo, White organic light-emitting diodes with fluorescent tube efficiency, Nature 459 (2009) 234–238. https://doi.org/10.1038/nature08003.

[6] H.-Y. Chen, J. Hou, S. Zhang, Y. Liang, G. Yang, Y. Yang, L. Yu, Y. Wu, G. Li, Polymer solar cells with enhanced open-circuit voltage and efficiency, Nat. Photonics 3 (2009) 649–653. https://doi.org/10.1038/nphoton.2009.192.
[7] M. Song, D.S. You, K. Lim, S. Park, S. Jung, C.S. Kim, D.-H. Kim, D.-G. Kim, J.-K. Kim, J. Park, Y.-C. Kang, J. Heo, S.-H. Jin, J.H. Park, J.-W. Kang, Highly efficient and bendable organic solar cells with solution-processed silver nanowire electrodes, Adv. Funct. Mater. 23 (2013) 4177–4184. https://doi.org/10.1002/adfm.201202646.
[8] N. Li, I. McCulloch, C.J. Brabec, Analyzing the efficiency, stability and cost potential for fullerene-free organic photovoltaics in one figure of merit, Energy Environ. Sci. 11 (2018) 1355-1361. https://doi.org/10.1039/C8EE00151K.
[9] K. Walzer, B. Maennig, M. Pfeiffer, K. Leo, Highly efficient organic devices based on electrically doped transport layers, Chem. Rev. 107 (2007) 1233–1271. https://doi.org/10.1021/cr050156n.
[10] A. Dai, Y. Zhou, A.L. Shu, S.K. Mohapatra, H. Wang, C. Fuentes-Hernandez, Y. Zhang, S. Barlow, Y.-L. Loo, S.R. Marder, B. Kippelen, A. Kahn, Enhanced charge-carrier injection and collection via lamination of doped polymer layers p-doped with a solution-processible molybdenum complex, Adv. Funct. Mater. 24 (2014) 2197–2204. https://doi.org/10.1002/adfm.201303232.
[11] H. Wang, C. Yu, Organic thermoelectrics: materials preparation, performance optimization, and device integration, Joule 3 (2019) 53–80. https://doi.org/10.1016/j.joule.2018.10.012.
[12] Y. Lu, J.-Y. Wang, J. Pei, Strategies to enhance the conductivity of n-type polymer thermoelectric materials, Chem. Mater. 31 (2019) 6412–6423. https://doi.org/10.1021/acs.chemmater.9b01422.
[13] P. Cheng, G. Li, X. Zhan, Y. Yang, Next-generation organic photovoltaics based on non-fullerene acceptors, Nat. Photonics 12 (2018) 131–142. https://doi.org/10.1038/s41566-018-0104-9.
[14] B. Lüssem, C.-M. Keum, D. Kasemann, B. Naab, Z. Bao, K. Leo, Doped organic transistors, Chem. Rev. 116 (2016) 13714–13751. https://doi.org/10.1021/acs.chemrev.6b00329.
[15] R. Kroon, D. Kiefer, D. Stegerer, L. Yu, M. Sommer, C. Müller, Polar side chains enhance processability, electrical conductivity, and thermal stability of a molecularly p-doped polythiophene, Adv. Mater. 29 (2017) 1700930. https://doi.org/10.1002/adma.201700930.
[16] H. Méndez, G. Heimel, S. Winkler, J. Frisch, A. Opitz, K. Sauer, B. Wegner, M. Oehzelt, C. Röthel, S. Duhm, D. Többens, N. Koch, I. Salzmann, Charge-transfer crystallites as molecular electrical dopants, Nat. Commun. 6 (2015) 8560. https://doi.org/10.1038/ncomms9560.
[17] D.T. Duong, C. Wang, E. Antono, M.F. Toney, A. Salleo, The chemical and structural origin of efficient p-type doping in P3HT, Org. Electron. 14 (2013) 1330–1336. https://doi.org/10.1016/j.orgel.2013.02.028.
[18] S. Olthof, W. Tress, R. Meerheim, B. Lüssem, K. Leo, Photoelectron spectroscopy study of systematically varied doping concentrations in an organic semiconductor layer using a molecular p-dopant, J. Appl. Phys. 106 (2009) 103711. https://doi.org/10.1063/1.3259436.
[19] F. Zhang, A. Kahn, Investigation of the high electron affinity molecular dopant F6-TCNNQ for hole-transport materials, Adv. Funct. Mater. 28 (2018) 1703780. https://doi.org/10.1002/adfm.201703780.
[20] I. Salzmann, G. Heimel, Toward a comprehensive understanding of molecular doping organic semiconductors (review), J. Electron Spectrosc. Relat. Phenom. 204 (2015) 208–222. https://doi.org/10.1016/j.elspec.2015.05.001.

[21] I.E. Jacobs, A.J. Moulé, Controlling molecular doping in organic semiconductors, Adv. Mater. 29 (2017) 1703063. https://doi.org/10.1002/adma.201703063.
[22] P. Reiser, L. Müller, V. Sivanesan, R. Lovrincic, S. Barlow, S.R. Marder, A. Pucci, W. Jaegermann, E. Mankel, S. Beck, Dopant diffusion in sequentially doped poly(3-hexylthiophene) studied by infrared and photoelectron spectroscopy, J. Phys. Chem. C 122 (2018) 14518–14527. https://doi.org/10.1021/acs.jpcc.8b02657.
[23] V. Vijayakumar, Y. Zhong, V. Untilova, M. Bahri, L. Herrmann, L. Biniek, N. Leclerc, M. Brinkmann, Bringing conducting polymers to high order: toward conductivities beyond 10^5 S cm^{-1} and thermoelectric power factors of 2 mW m^{-1} K^{-2}, Adv. Energy Mater. 9 (2019) 1900266. https://doi.org/10.1002/aenm.201900266.
[24] K. Norrman, M.V. Madsen, S.A. Gevorgyan, F.C. Krebs, Degradation patterns in water and oxygen of an inverted polymer solar cell, J. Am. Chem. Soc. 132 (2010) 16883–16892. https://doi.org/10.1021/ja106299g.
[25] W.R. Mateker, M.D. McGehee, Progress in understanding degradation mechanisms and improving stability in organic photovoltaics, Adv. Mater. 29 (2017) 1603940. https://doi.org/10.1002/adma.201603940.
[26] M. Nikolka, I. Nasrallah, B. Rose, M.K. Ravva, K. Broch, A. Sadhanala, D. Harkin, J. Charmet, M. Hurhangee, A. Brown, S. Illig, P. Too, J. Jongman, I. McCulloch, J.-L. Bredas, H. Sirringhaus, High operational and environmental stability of high-mobility conjugated polymer field-effect transistors through the use of molecular additives, Nat. Mater. 16 (2017) 356–362. https://doi.org/10.1038/nmat4785.
[27] D.M. de Leeuw, M.M.J. Simenon, A.R. Brown, R.E.F. Einerhand, Stability of n-type doped conducting polymers and consequences for polymeric microelectronic devices, Synth. Met. 87 (1997) 53–59. https://doi.org/10.1016/S0379-6779(97)80097-5.
[28] H. Usta, C. Risko, Z. Wang, H. Huang, M.K. Deliomeroglu, A. Zhukhovitskiy, A. Facchetti, T.J. Marks, Design, synthesis, and characterization of ladder-type molecules and polymers. Air-stable, solution-processable n-channel and ambipolar semiconductors for thin-film transistors via experiment and theory, J. Am. Chem. Soc. 131 (2009) 5586–5608. https://doi.org/10.1021/ja809555c.
[29] H.T. Nicolai, M. Kuik, G. a. H. Wetzelaer, B. de Boer, C. Campbell, C. Risko, J.L. Brédas, P.W.M. Blom, Unification of trap-limited electron transport in semiconducting polymers, Nat. Mater. 11 (2012) 882–887. https://doi.org/10.1038/nmat3384.
[30] M.L. Tietze, B.D. Rose, M. Schwarze, A. Fischer, S. Runge, J. Blochwitz-Nimoth, B. Lüssem, K. Leo, J.-L. Brédas, Passivation of molecular n-doping: exploring the limits of air stability, Adv. Funct. Mater. 26 (2016) 3730–3737. https://doi.org/10.1002/adfm.201505092.
[31] M.L. Tietze, F. Wölzl, T. Menke, A. Fischer, M. Riede, K. Leo, B. Lüssem, Self-passivation of molecular n-type doping during air exposure using a highly efficient air-instable dopant, Phys. Status Solidi A 210 (2013) 2188–2198. https://doi.org/10.1002/pssa.201330049.
[32] J.-M. Zhuo, L.-H. Zhao, R.-Q. Png, L.-Y. Wong, P.-J. Chia, J.-C. Tang, S. Sivaramakrishnan, M. Zhou, E.C.-W. Ou, S.-J. Chua, W.-S. Sim, L.-L. Chua, P.K.-H. Ho, Direct spectroscopic evidence for a photodoping mechanism in polythiophene and poly(bithiophene-alt-thienothiophene) organic semiconductor thin films involving oxygen and sorbed moisture, Adv. Mater. 21 (2009) 4747–4752. https://doi.org/10.1002/adma.200901120.
[33] S.K. Mohapatra, Y. Zhang, B. Sandhu, M.S. Fonari, T.V. Timofeeva, S.R. Marder, S. Barlow, Synthesis, characterization, and crystal structures of molybdenum complexes of unsymmetrical electron-poor dithiolene ligands, Polyhedron 116 (2016) 88–95. https://doi.org/10.1016/j.poly.2016.04.025.

[34] A. Dai, Creating highly efficient carrier injection or collection contacts via soft contact transfer lamination of p-doped interlayers, Ph.D. Thesis, Princeton University, 2015. http://arks.princeton.edu/ark:/88435/dsp01sq87bx003.
[35] J. Euvrard, A. Revaux, P.-A. Bayle, M. Bardet, D. Vuillaume, A. Kahn, The formation of polymer-dopant aggregates as a possible origin of limited doping efficiency at high dopant concentration, Org. Electron. 53 (2018) 135–140. https://doi.org/10.1016/j.orgel.2017.11.020.
[36] J. Euvrard, A. Revaux, S.S. Nobre, A. Kahn, D. Vuillaume, Toward a better understanding of the doping mechanism involved in Mo(tfd-$COCF_3$)$_3$ doped PBDTTT-c, J. Appl. Phys. 123 (2018) 225501. https://doi.org/10.1063/1.5029810.
[37] C.M. Cardona, W. Li, A.E. Kaifer, D. Stockdale, G.C. Bazan, Electrochemical Considerations for determining absolute frontier orbital energy levels of conjugated polymers for solar cell applications, Adv. Mater. 23 (2011) 2367–2371. https://doi.org/10.1002/adma.201004554.
[38] S.K. Lee, Y. Zu, A. Herrmann, Y. Geerts, K. Müllen, A.J. Bard, Electrochemistry, spectroscopy and electrogenerated chemiluminescence of perylene, terrylene, and quaterrylene diimides in aprotic solution, J. Am. Chem. Soc. 121 (1999) 3513–3520. https://doi.org/10.1021/ja984188m.
[39] J. Li, I. Duchemin, O.M. Roscioni, P. Friederich, M. Anderson, E. Da Como, G. Kociok-Köhn, W. Wenzel, C. Zannoni, D. Beljonne, X. Blase, G. D'Avino, Host dependence of the electron affinity of molecular dopants, Mater. Horiz. 6 (2019) 107–114. https://doi.org/10.1039/C8MH00921J.
[40] Y. Wang, M. Nakano, T. Michinobu, Y. Kiyota, T. Mori, K. Takimiya, Naphthodithiophenediimide–benzobisthiadiazole-based polymers: versatile n-type materials for field-effect transistors and thermoelectric devices, Macromolecules 50 (2017) 857–864. https://doi.org/10.1021/acs.macromol.6b02313.
[41] R. Fujimoto, S. Watanabe, Y. Yamashita, J. Tsurumi, H. Matsui, T. Kushida, C. Mitsui, H.T. Yi, V. Podzorov, J. Takeya, Control of molecular doping in conjugated polymers by thermal annealing, Org. Electron. 47 (2017) 139–146. https://doi.org/10.1016/j.orgel.2017.05.019.
[42] H. Hase, K. O'Neill, J. Frisch, A. Opitz, N. Koch, I. Salzmann, Unraveling the microstructure of molecularly doped poly(3-hexylthiophene) by thermally induced dedoping, J. Phys. Chem. C 122 (2018) 25893-25899. https://doi.org/10.1021/acs.jpcc.8b08591.
[43] P. Pingel, L. Zhu, K.S. Park, J.-O. Vogel, S. Janietz, E.-G. Kim, J.P. Rabe, J.-L. Brédas, N. Koch, Charge-transfer localization in molecularly doped thiophene-based donor polymers, J. Phys. Chem. Lett. 1 (2010) 2037–2041. https://doi.org/10.1021/jz100492c.
[44] D. Huang, H. Yao, Y. Cui, Y. Zou, F. Zhang, C. Wang, H. Shen, W. Jin, J. Zhu, Y. Diao, W. Xu, C. Di, D. Zhu, Conjugated-backbone effect of organic small molecules for n-type thermoelectric materials with ZT over 0.2, J. Am. Chem. Soc. 139 (2017) 13013–13023. https://doi.org/10.1021/jacs.7b05344.
[45] C. Cobet, J. Gasiorowski, R. Menon, K. Hingerl, S. Schlager, M.S. White, H. Neugebauer, N.S. Sariciftci, P. Stadler, Influence of molecular designs on polaronic and vibrational transitions in a conjugated push-pull copolymer, Sci. Rep. 6 (2016) 35096. https://doi.org/10.1038/srep35096.
[46] S. Winkler, P. Amsalem, J. Frisch, M. Oehzelt, G. Heimel, N. Koch, Probing the energy levels in hole-doped molecular semiconductors, Mater. Horiz. 2 (2015) 427–433. https://doi.org/10.1039/C5MH00023H.
[47] G. Heimel, The optical signature of charges in conjugated polymers, ACS Cent. Sci. 2 (2016) 309–315. https://doi.org/10.1021/acscentsci.6b00073.

[48] J. Hou, H.-Y. Chen, S. Zhang, R.I. Chen, Y. Yang, Y. Wu, G. Li, Synthesis of a low band gap polymer and its application in highly efficient polymer solar cells, J. Am. Chem. Soc. 131 (2009) 15586–15587. https://doi.org/10.1021/ja9064975.
[49] Y. Liang, Y. Wu, D. Feng, S.-T. Tsai, H.-J. Son, G. Li, L. Yu, Development of new semiconducting polymers for high performance solar cells, J. Am. Chem. Soc. 131 (2009) 56–57. https://doi.org/10.1021/ja808373p.
[50] C. Wang, D.T. Duong, K. Vandewal, J. Rivnay, A. Salleo, Optical measurement of doping efficiency in poly(3-hexylthiophene) solutions and thin films, Phys. Rev. B 91 (2015) 085205. https://doi.org/10.1103/PhysRevB.91.085205.
[51] K. Tang, F.M. McFarland, S. Travis, J. Lim, J.D. Azoulay, S. Guo, Aggregation of P3HT as a preferred pathway for its chemical doping with F4-TCNQ, Chem. Commun. 54 (2018) 11925–11928. https://doi.org/10.1039/C8CC05472J.
[52] F.M. McFarland, C.M. Ellis, S. Guo, The aggregation of poly(3-hexylthiophene) into nanowires: with and without chemical doping, J. Phys. Chem. C 121 (2017) 4740–4746. https://doi.org/10.1021/acs.jpcc.7b00816.
[53] D.T. Duong, H. Phan, D. Hanifi, P.S. Jo, T.-Q. Nguyen, A. Salleo, Direct Observation of doping Sites in temperature-controlled, p-doped P3HT thin films by conducting atomic force microscopy, Adv. Mater. 26 (2014) 6069–6073. https://doi.org/10.1002/adma.201402015.
[54] D. Kiefer, R. Kroon, A.I. Hofmann, H. Sun, X. Liu, A. Giovannitti, D. Stegerer, A. Cano, J. Hynynen, L. Yu, Y. Zhang, D. Nai, T.F. Harrelson, M. Sommer, A.J. Moulé, M. Kemerink, S.R. Marder, I. McCulloch, M. Fahlman, S. Fabiano, C. Müller, Double doping of conjugated polymers with monomer molecular dopants, Nat. Mater. 18 (2019) 149–155. https://doi.org/10.1038/s41563-018-0263-6.
[55] J.H. Oh, Y.-S. Sun, R. Schmidt, M.F. Toney, D. Nordlund, M. Könemann, F. Würthner, Z. Bao, Interplay between energetic and kinetic factors on the ambient stability of n-channel organic transistors based on perylene diimide derivatives, Chem. Mater. 21 (2009) 5508–5518. https://doi.org/10.1021/cm902531d.
[56] H.-H. Liao, C.-M. Yang, C.-C. Liu, S.-F. Horng, H.-F. Meng, J.-T. Shy, Dynamics and reversibility of oxygen doping and de-doping for conjugated polymer, J. Appl. Phys. 103 (2008) 104506. https://doi.org/10.1063/1.2917419.
[57] I.E. Jacobs, F. Wang, N. Hafezi, C. Medina-Plaza, T.F. Harrelson, J. Li, M.P. Augustine, M. Mascal, A.J. Moulé, Quantitative dedoping of conductive polymers, Chem. Mater. 29 (2017) 832–841. https://doi.org/10.1021/acs.chemmater.6b04880.
[58] D. Kiefer, A. Giovannitti, H. Sun, T. Biskup, A. Hofmann, M. Koopmans, C. Cendra, S. Weber, L.J. Anton Koster, E. Olsson, J. Rivnay, S. Fabiano, I. McCulloch, C. Müller, Enhanced n-doping efficiency of a naphthalenediimide-based copolymer through polar side chains for organic thermoelectrics, ACS Energy Lett. 3 (2018) 278–285. https://doi.org/10.1021/acsenergylett.7b01146.
[59] Y. Qi, T. Sajoto, M. Kröger, A.M. Kandabarow, W. Park, S. Barlow, E.-G. Kim, L. Wielunski, L.C. Feldman, R.A. Bartynski, J.-L. Brédas, S.R. Marder, A. Kahn, A molybdenum dithiolene complex as p-dopant for hole-transport materials: a multitechnique experimental and theoretical investigation, Chem. Mater. 22 (2010) 524–531. https://doi.org/10.1021/cm9031623.
[60] N.H. Turner, A.M. Single, Determination of peak positions and areas from wide-scan XPS spectra, Surf. Interface Anal. 15 (1990) 215–222. https://doi.org/10.1002/sia.740150305.
[61] J. Richard, A. Benayad, J.-F. Colin, S. Martinet, Charge transfer mechanism into the chevrel phase Mo_6S_8 during Mg intercalation, J. Phys. Chem. C. 121 (2017) 17096–17103. https://doi.org/10.1021/acs.jpcc.7b03979.

[62] R. Eisenberg, H.B. Gray, Noninnocence in metal complexes: a dithiolene dawn, Inorg. Chem. 50 (2011) 9741–9751. https://doi.org/10.1021/ic2011748.
[63] C.D. Wagner, W.M. Riggs, L.E. Davis, J.F. Moulder, G.E. Muilenburg, Handbook of X-ray Photoelectron Spectroscopy, Perkin-Elmer, Eden Prairie, MN, 1979. https://doi.org/10.1002/sia.740030412.
[64] T.H. Fleisch, G.J. Mains, An XPS study of the UV reduction and photochromism of MoO_3 and WO_3, J. Chem. Phys. 76 (1982) 780–786. https://doi.org/10.1063/1.443047.
[65] A. Dupé, M.E. Judmaier, F. Belaj, K. Zangger, N.C. Mösch-Zanetti, Activation of molecular oxygen by a molybdenum complex for catalytic oxidation, Dalton Trans. 44 (2015) 20514–20522. https://doi.org/10.1039/C5DT02931G.
[66] R. Hille, The molybdenum oxotransferases and related enzymes, Dalton Trans. 42 (2013) 3029–3042. https://doi.org/10.1039/C2DT32376A.

Material	$S2s_{dop}$	$S2s_{pol}$	C-S		Mo-S-C		Mo^{4+}		$Mo^{4+/5+}$		Mo^{6+}	
			$S2p_{3/2}$	$S2p_{1/2}$	$S2p_{3/2}$	$S2p_{1/2}$	$Mo3d_{5/2}$	$Mo3d_{3/2}$	$Mo3d_{5/2}$	$Mo3d_{3/2}$	$Mo3d_{5/2}$	$Mo3d_{3/2}$
Pristine PBDTTT-c	–	–	163.7	164.9	–	–	–	–	–	–	–	–
Pristine Mo(tfd-$COCF_3$)$_3$	226.7	–	–	–	162.3	163.5	229.1	232.3	231.3	234.4	–	–
PBDTTT-c: Mo(tfd-$COCF_3$)$_3$ **before air exposure**	226.7	228.1	163.7	164.9	162.3	163.5	229.4	232.6	**231.0**	**234.1**	**–**	**–**
PBDTTT-c: Mo(tfd-$COCF_3$)$_3$ **after air exposure**	226.7	228.1	163.7	164.9	162.3 **(vanished)**	163.5	230.0	233.1	**–**	**–**	**232.0**	**235.1**

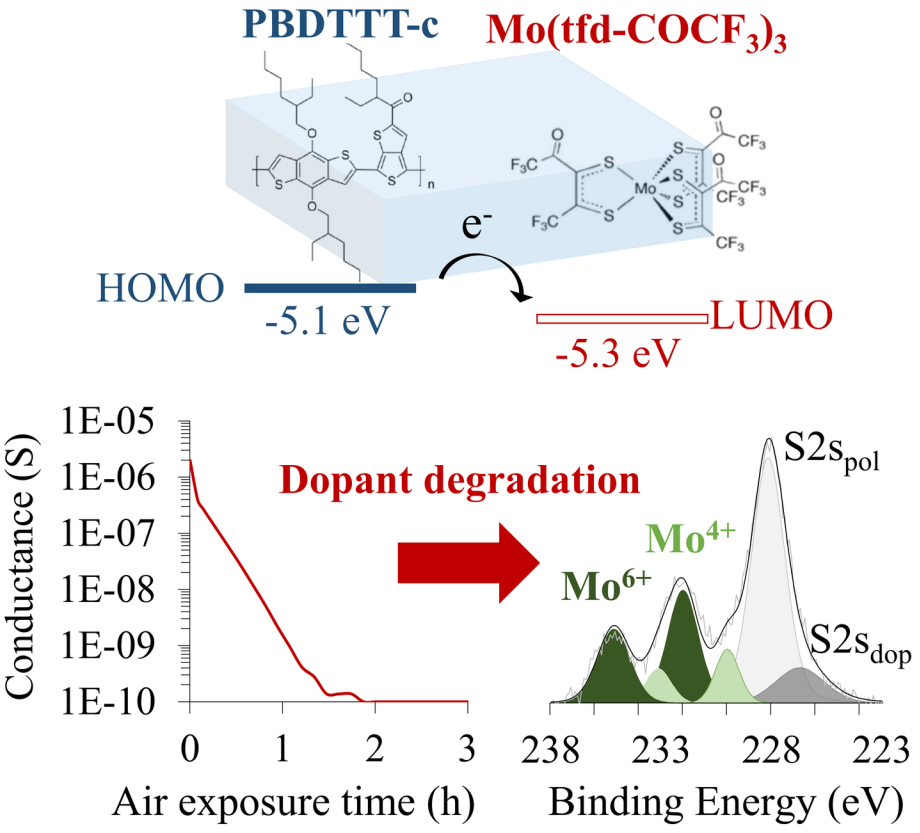
PBDTTT-c
Mo(tfd-COCF3)3
e-
HOMO
-5.1 eV
LUMO
-5.3 eV
Dopant degradation
Conductance (S)
1E-05
1E-06
1E-07
1E-08
1E-09
1E-10
0
1
2
3
Air exposure time (h)
S2spol
Mo4+
Mo6+
S2sdop
238
233
228
223
Binding Energy (eV)